2017 SCEC Proposal Report #17133

Imaging sharp lateral velocity gradients using scattered waves on dense arrays: faults and basin edges

Principal Investigator

Zhongwen Zhan

Seismological Laboratory, California Institute of Technology, Pasadena, CA 91125

zwzhan@gps.caltech.edu

Postdoc

Chunquan Yu

Seismological Laboratory, California Institute of Technology, Pasadena, CA 91125

yucq@gps.caltech.edu

09 June 2018

Summary

Sharp lateral velocity contrasts often exist across major faults, at basin edges, or along other geological features. While the SCEC community velocity models continue to improve in resolution, sharp velocity gradients remain difficult to image, due to limitations in data coverage and damping in inversions. Here, we analyzed broadband waveforms recorded by the Southern California Seismic Network and observed strong body-to-surface wave scattering for various teleseismic incident wave types. We focused our study on strongly scattered Love waves following the arrival of teleseismic *SH* wave. These scattered Love waves travel approximately in the same (azimuthal) direction as the incident *SH* wave at a dominant period of ~10 s but at an apparent velocity of ~3.6 km/s as compared to the ~11 km/s for the *SH* wave. Back-projection suggests that this strong scattering is associated with pronounced bathymetric relief in the Southern California Continental Borderland, in particular the Patton Escarpment. Finite-difference simulations using a simplified 2-D bathymetric and crustal model are able to predict the arrival times and amplitudes of major scatterers. The modeling suggests a relatively low shear wave velocity in the Continental Borderland.

Broader Impacts

Our study shows that scattered waves could be used to calibrate/update existing SCEC community velocity models, e.g. CVM-S4.26 (*Lee et al., 2014*) and CVM-H15.1.0 (*Shaw et al., 2015*), in particular across the California Continental Borderland, where stations are sparse. Such practice may enable to more precise offshore earthquake locations as well as improved seismic hazard assessment through, for example, CyberShake seismic hazard model calculations (*Graves et al., 2011*). The methodology in this study can essentially be applied to other seismic arrays, such as the EarthScope Transportable Array, to image potential scatterers on a broader scale.

Technical description

1. Observation of strong body-to-surface wave scattering

Figure 1a shows transverse-component waveforms for a deep focal event occurred in the Tonga-Kermadec-Fiji subduction zone (25.24^{o}S, 179.41^{o}E; 535 km depth; M_w 6.5; 2007-10-05 07:17:54.7 UTC). Seismic waveforms are sorted by epicentral distances (reduced by 83.96^{o} at the reference station) and only stations within a 2^{o}-radius area centered at CI.MWC are shown. The direct *SH* phase arrives between -20 s and 20 s (reduced by 1281.4 s at the reference station) with a horizontal slowness ~10 s/^{o} (or an apparent velocity ~11.1 km/s), consistent with the theoretical prediction from *ak135* (Kennett et al., 1995). Following the direct *SH* phase arrival, there are at least two additional coherent phases: a high amplitude coherent phase arrival followed by a weaker phase arrival at ~70 s and ~45 s (at the reference station), respectively ("L1" and "L2" in **Figure 1a**). These two phases travel at a much slower apparent velocity with no clear amplitude decay with distance. Similar phases are also consistently observed for other events that originate near the Tonga-Kermadec-Fiji source region. We infer that scattering off near-receiver heterogeneities may cause the observed phases that follow the *SH* arrival.

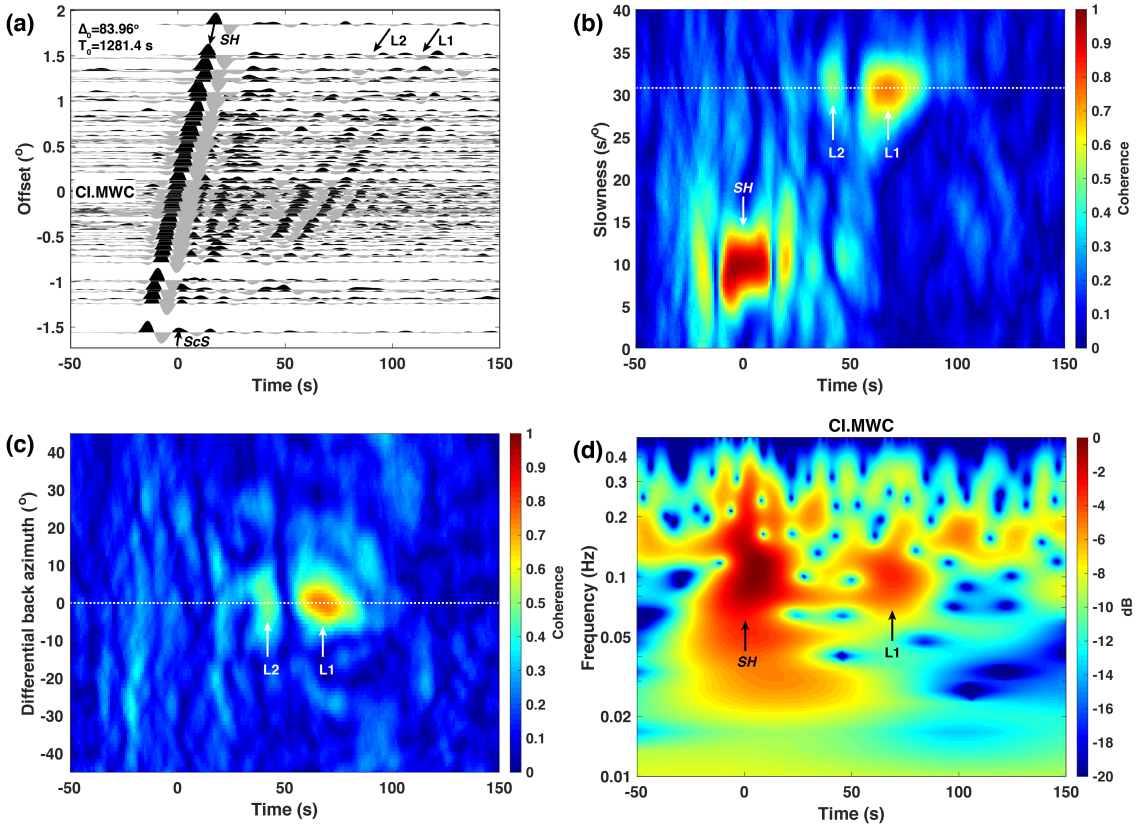

Figure 1. *Waveform analysis of a deep M_w 6.5 event from the Tonga-Kermadec-Fiji subduction zone. (a) Tangential-component seismograms (proportional to ground velocity) sorted by distance to the earthquake source. Seismograms are bandpass filtered between 0.02 and 0.1 Hz with a two-pass Butterworth filter. Time and distance are reduced by the SH arrival and the epicentral distance at the reference station CI.MWC, respectively. "L1" and "L2" are two scattered waves. (b) Slowness-time cross section of phase coherence across the maximum coherence point of scattered waves (slowness=31 s/°, differential back azimuth=0°). (c) same as (b) but for a back azimuth-time cross section. (d) Time-frequency analysis of the raw seismogram at station CI.MWC. Note both direct SH and "L1" have a dominant central frequency ~0.1 Hz.*

2. Locations of scatterers

We use back-projection to locate the sources of scattered Love waves. The apparent source wavelet is subtracted and deconvolved from each trace. Residual traces are then shifted and stacked in a 1° radius bin around each station for all back azimuths, assuming a constant horizontal slowness 31 s/° (estimated from the entire array; **Figure 1b**). The envelopes of stacked traces (normalized by the *SH*-wave amplitude) are finally back-projected to estimate the source of the scattered phases.

The strongest scatterer "L1" is fit to a linear feature roughly perpendicular to the wave propagation direction and parallel to the western edge of the Continental Borderland – the Patton Escarpment (**Figure 2**), which is the most prominent lateral heterogeneity both at the surface and near the crustal root in this region. Aligning the strongest scatterer to the

Patton Escarpment leads to a best fitting Love wave velocity of ~3.1 km/s across the Continental Borderland. The slightly weaker scatterer "L2" (**Figure 1a**) is generated within the Continental Borderland; the source of this scattered arrival is most likely associated with borderland basins, such as the Santa Cruz Basin and the San Nicolas Basin, where bathymetric relief is also significant (**Figure 2**).

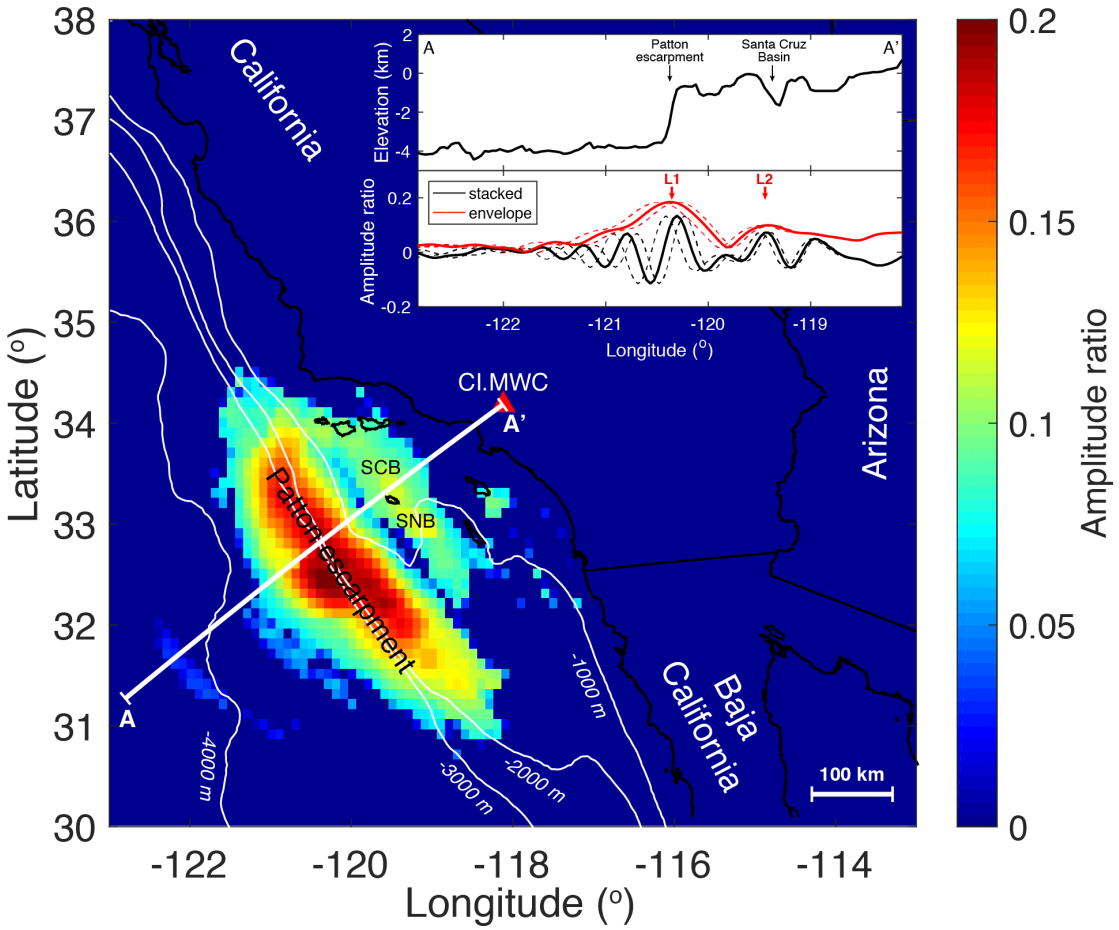

Figure 2. *Back-projection of scattered wave envelope for the selected Tonga-Kermadec-Fiji event. Amplitude is normalized by that of the direct SH phase and muted if the phase coherence is not significant. Constant Love wave velocities 3.1 km/s and 3.6 km/s are used for the region to the west and east of the coast line, respectively. Inset is a comparison between topography and back-projected waveforms (black for stacked waveform, red for envelope) along AA' profile. Dashed lines show perturbations of back-projected waveforms assuming a ±0.1 km/s difference in the Love wave velocity of the Continental Borderland. Envelope peaks correlate with pronounced topographic relief at the Patton Escarpment and the Santa Cruz Basin.*

3. 2-D finite-difference waveform modeling

To better understand the scattering process, we further perform finite-difference simulations and compare synthetic waveforms with observations. Since scatterers align roughly perpendicular to the wave propagation direction, 2-D models are adequate for our purpose. Our global 2-D finite-difference simulation is based on the method of *Li et al.*

(2014). Our synthetic waveforms capture the salient features of the scattered wavefield. For the scattered wave from the Patton Escarpment ("L1" in **Figure 3b**), both the arrival times and amplitudes are well predicted. We note that synthetic waveforms do not fully reproduce scattered wavefield after "L1", which could be due to either *ScS* scattering or additional structural heterogeneities to the west of the Patton Escarpment, such as the San Juan Seamount. For scatterers from the Santa Cruz Basin ("L2" in **Figure 3b**), the synthetics generally explain the arrival times but under predict the amplitudes. The under prediction of the amplitudes might be due to the amplification effect from low-velocity sediments in the Santa Cruz Basin, which are not included in our model.

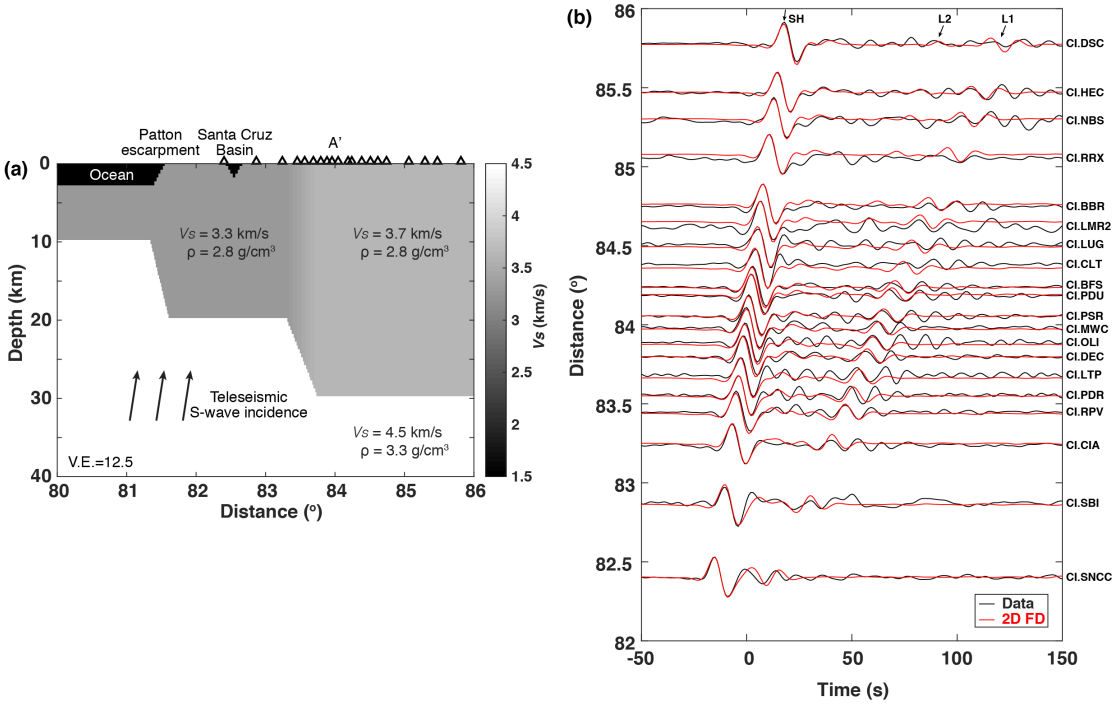

Figure 3. *2D finite-difference waveform modeling of SH-to-Love wave scattering. (a) A simplified Vs and density model near receivers. The topography is simplified from that along profile AA' (**Figure 2**; extended further to the northeast). Crustal thickness is based on Miller (2002). (b) A direct comparison of observed and synthetic waveforms for selected stations along profile AA'. Note for scattered Love waves from the Patton Escarpment ("L1") both the arrival times and amplitudes are well modeled.*

Presentation and publication

Postdoc Chunquan Yu presented the work at 2017 SCEC annual meeting. The manuscript on the body-to-surface wave scattering around Southern California is published as (*Yu et al., 2017*) in *Geophysical Research Letters*.

References

Graves, R., T. H. Jordan, S. Callaghan, E. Deelman, E. Field, G. Juve, C. Kesselman, P. Maechling, G. Mehta, and K. Milner (2011), CyberShake: A physics-based seismic hazard model for southern California, *Pure Appl. Geophys.*, *168*(3-4), 367-381.

Kennett, B., E. Engdahl, and R. Buland (1995), Constraints on seismic velocities in the Earth from traveltimes, *Geophys. J. Int.*, *122*(1), 108-124.

Li, D., D. Helmberger, R. W. Clayton, and D. Sun (2014), Global synthetic seismograms using a 2-D finite-difference method, *Geophys. J. Int.*, *197*(2), 1166-1183.

Miller, K. C. (2002), Geophysical evidence for Miocene extension and mafic magmatic addition in the California Continental Borderland, *Geol. Soc. Am. Bull.*, *114*(4), 497-512.

Shaw, John H., Plesch, Andreas, Tape, Carl, Suess, M. Peter, Jordan, Thomas H., Ely, Geoffrey, Hauksson, Egill, Tromp, Jeroen, Tanimoto, Toshiro, Graves, Robert, Olsen, Kim, Nicholson, Craig, Maechling, Philip J., Rivero, Carlos, Lovely, Peter, Brankman, Charles M., Munster, Jason (2015) Unified Structural Representation of the southern California crust and upper mantle, Earth and Planetary Science Letters, V. 415, Num. 0, p.1-15,

Yu, C., Zhan, Z., Hauksson, E., & Cochran, E. (2017). Strong SH-to-Love Wave Scattering off the Southern California Continental Borderland. *Geophysical Research Letters*, 2017GL075213. https://doi.org/10.1002/2017GL075213.